Nano Research 2018, 11(6): 3164–3174
https://doi.org/10.1007/s12274-017-1721-1
Research Article
ISSN 1998-0124
CN 11-5974/O4

A strategy for accurate detection of glucose in human serum and whole blood based on an upconversion nanoparticles-polydopamine nanosystem

Yan Liu[1,2], Datao Tu[1], Wei Zheng[1] (✉), Lianyu Lu[1], Wenwu You[1,2], Shanyong Zhou[1], Ping Huang[1], Renfu Li[1], and Xueyuan Chen[1,2] (✉)

[1] *CAS Key Laboratory of Design and Assembly of Functional Nanostructures, and Fujian Key Laboratory of Nanomaterials, Fujian Institute of Research on the Structure of Matter, Chinese Academy of Sciences, Fuzhou 350002, China*
[2] *University of Chinese Academy of Sciences, Beijing 100049, China*

Received: 17 April 2017
Revised: 2 June 2017
Accepted: 10 June 2017

KEYWORDS
upconversion nanoparticles,
polydopamine,
Förster resonance energy transfer,
blood glucose,
bioassay

ABSTRACT

The accurate detection of blood glucose is of critical importance in the diagnosis and management of diabetes and its complications. Herein, we report a novel strategy based on an upconversion nanoparticles-polydopamine (UCNPs-PDA) nanosystem for the accurate detection of glucose in human serum and whole blood through a simple blending of test samples with ligand-free UCNPs, dopamine, and glucose oxidase (GOx). Owing to the high affinity of lanthanide ions exposed on the surface of ligand-free UCNPs, dopamine monomers could spontaneously attach to the UCNPs and further polymerize to form a PDA shell, resulting in a remarkable upconversion luminescence (UCL) quenching (97.4%) of UCNPs under 980-nm excitation. Such UCL quenching can be effectively inhibited by H_2O_2 produced from the GOx/glucose enzymatic reaction, thus enabling the detection of H_2O_2 or glucose based on the UCL quenching/inhibition bioassay. Owing to the highly sensitive UCL response and background-free interference of the UCNPs-PDA nanosystem, we achieved a sensitive, selective, and high-throughput bioassay for glucose in human serum and whole blood, thereby revealing the great potential of the UCNPs-PDA nanosystem for the accurate detection of blood glucose or other H_2O_2-generated biomolecules in clinical bioassays.

1 Introduction

Blood glucose is the primary energy source for cells *in vivo*, and levels outside the normal range may be an indicator of a medical condition[1]. A persistently high level of blood glucose indicates diabetes mellitus, which is one of the most common metabolic diseases and can cause many serious complications such as high

Address correspondence to Wei Zheng, zhengwei@fjirsm.ac.cn; Xueyuan Chen, xchen@fjirsm.ac.cn

blood pressure, kidney failure, blindness, stroke, and heart attack [2–4]. Accurate detection and monitoring of blood glucose is of great importance in the clinical diagnosis and management of diabetes and its complications [5–7]. Among diverse glucose detection methods, the fluorescence analysis of H_2O_2 produced from the glucose oxidase (GOx)/glucose enzymatic reaction is considered extremely effective [8–12]. However, conventional fluorescence bioprobes such as organic dyes and quantum dots usually suffer from the disadvantages of background interference from biological autofluorescence, low photochemical stability, and high toxicity [13–15]. Thus, those probes are not ideal for applications in glucose detection, especially for the accurate detection of glucose in human serum or whole blood.

As a new generation of luminescent nanoprobes, lanthanide (Ln^{3+})-doped upconversion nanoparticles (UCNPs) have evoked considerable interest in the field of biomedicine owing to their excellent physicochemical properties, such as high photochemical stability, low toxicity, and absence of autofluorescence in biological specimens under near-infrared (NIR) excitation [16–24]. Therefore, they are ideal bioprobe candidates for glucose detection in complex biological samples. Recently, based on UCNPs, several Förster resonance energy transfer (FRET)-based bioassay systems have been proposed for glucose detection [25–28]. Nonetheless, these bioassay systems necessitate complicated operations involved in the surface modification of UCNP energy donors or the specially designed synthesis of H_2O_2-responsive energy acceptors, which would undoubtedly decrease the convenience and increase the cost. Moreover, an interlayer was imposed between the donor and acceptor during the surface modification of UCNP donors, which is unfavorable for the distance-dependent FRET and would inevitably decrease the detection sensitivity. Therefore, it is highly essential to develop a facile, sensitive, and cost-effective UC-FRET bioassay system for the accurate detection of blood glucose levels for the clinical diagnosis and management of diabetes and its complications.

As one of the most important neurotransmitters and a mimic of mussel adhesive proteins, dopamine (DA) can spontaneously deposit on virtually any surface and further polymerize to form a conformal polydopamine (PDA) layer [29–31]. PDA exhibits high absorbance in the visible spectral region, and thus could serve as an efficient energy quencher for UCNPs [32–34]. Based on the UCNPs-PDA nanosystem, herein, we report a facile and cost-effective strategy for the sensitive and selective detection of glucose in human serum and whole blood through a simple blending of test samples with ligand-free UCNPs, DA, and GOx. The quenching effect of PDA on the upconversion luminescence (UCL) and the inhibition effect of H_2O_2 on the UCL quenching of the UCNPs-PDA nanosystem were systematically investigated through UCL spectroscopy under 980-nm excitation. High-throughput glucose detection in a buffer solution, human serum, and whole blood is demonstrated herein, based on a customized UCL biodetection system coupled in a multimodal microplate reader (Synergy 4, BioTeK).

2 Experimental

2.1 Chemicals and materials

$Y(CH_3COO)_3{\cdot}4H_2O$ (99.99%), $Yb(CH_3COO)_3{\cdot}4H_2O$ (99.99%), $Er(CH_3COO)_3{\cdot}4H_2O$ (99.99%), NaOH, NH_4F, Tris(hydroxymethyl)aminomethane (Tris), hydrochloric acid, cyclohexane, and ethanol were purchased from Sinopharm Chemical Reagent Co., Ltd. (Shanghai, China). Glucose, fructose, galactose, sucrose, H_2O_2 solution (30 wt.%), DA chloride, oleic acid (OA), oleylamine (OM), and 1-octadecence (ODE) were purchased from Sigma-Aldrich (China). Glutathione (GSH), cysteine (Cys), human serum albumin (HSA), bovine serum albumin (BSA), amino acids, and other chemical reagents were purchased from Aladdin Reagent Co., Ltd. (Shanghai, China). All chemicals were used as received without further purification, and distilled water was used throughout the experiments.

2.2 Synthesis of oleate-capped $NaYF_4$:Yb/Er UCNPs

Oleate-capped $NaYF_4$:Yb/Er UCNPs were synthesized through a high-temperature co-precipitation method [35]. Briefly, $Y(CH_3COO)_3{\cdot}4H_2O$ (0.80 mmol), $Yb(CH_3COO)_3{\cdot}4H_2O$ (0.18 mmol), and $Er(CH_3COO)_3{\cdot}4H_2O$ (0.02 mmol) were mixed with 6 mL of OA and 15 mL

of ODE in a 100-mL three-neck round-bottom flask. The resulting mixture was heated to 160 ℃ under N_2 flow with constant stirring for 30 min to form a clear solution, and then cooled down to room temperature (RT). Thereafter, 10 mL of methanol solution containing 4 mmol of NH_4F and 2.5 mmol of NaOH was added and the solution was stirred at 60 ℃ for 1 h to remove methanol. After methanol was evaporated, the resulting solution was heated to 300 ℃ under N_2 flow with vigorous stirring for 1 h, and then cooled down to RT. The obtained UCNPs were precipitated by adding ethanol, collected by centrifuging, washed with ethanol several times, and finally re-dispersed in 5 mL of cyclohexane.

2.3 Synthesis of ligand-free $NaYF_4$:Yb/Er UCNPs

Ligand-free $NaYF_4$:Yb/Er UCNPs were obtained by removing the surface ligands of their oleate-capped counterparts through acid treatment [36]. Briefly, 30 mg of the oleate-capped $NaYF_4$:Yb/Er UCNPs were dispersed in 15 mL of acidic ethanol solution (pH = 1) and ultrasonicated for 30 min to remove the surface ligands. Subsequently, the UCNPs were collected via centrifugation at 11,800 *g* for 20 min. The product was further purified by adding an acidic ethanol solution (pH = 4), and the mixture was ultrasonicated for another 30 min at RT. The resulting products were washed with ethanol several times and finally re-dispersed in distilled water.

2.4 Synthesis of PDA-capped $NaYF_4$:Yb/Er UCNPs

PDA-capped $NaYF_4$:Yb/Er UCNPs were synthesized via a simple mixing of ligand-free UCNPs and DA monomers, which can spontaneously attach onto the surface of ligand-free UCNPs and further polymerize to form a PDA shell. Briefly, ligand-free $NaYF_4$:Yb/Er UCNPs (0.4 mg·mL^{-1}) were mixed with different amounts (0–1 mM) of DA in 200 μL of Tris-HCl buffer solution (10 mM, pH 8.5). The mixture was then incubated at 37 ℃ for 2 h under gentle mixing. The sample solution was extracted for structure and optical property characterizations to investigate the evolution of the size, morphology, absorption, and UCL properties of the resulting products on DA concentration and incubation time.

2.5 Absorption and UCL measurement of the UCNPs/DA/H_2O_2 solution

Typically, ligand-free UCNPs (0.4 mg·mL^{-1}) and DA (500 μM) were mixed with different amounts (0–250 μM) of H_2O_2 in 200 μL of Tris-HCl buffer solution in a 96-well microplate. After incubation at 37 ℃ for 1 h, 10 μL of HCl solution (120 mM) was added into each well to terminate the DA polymerization. The microplate was then subjected to UV–Vis absorption and UCL measurement under 980-nm excitation on a customized UCL biodetection system coupled in a multimodal microplate reader (Synergy 4, BioTeK).

2.6 Glucose detection based on the UCNPs-PDA nanosystem

For glucose detection in Tris-HCl buffer solution, ligand-free UCNPs (0.4 mg·mL^{-1}), DA (500 μM), and GOx (0.05 mg·mL^{-1}) were mixed with different amounts (0–300 μM) of glucose in 200 μL of Tris-HCl buffer solution (10 mM, pH = 8.5) in a 96-well microplate. After incubation at 37 ℃ for 1 h, the microplate was subjected to UCL measurement under 980-nm excitation. For comparison, control experiments were conducted by replacing glucose with other interfering analytes, including sugars, proteins, L-amino acids, and metal ions, under otherwise identical conditions.

For glucose detection in human serum and whole blood, a calibration curve for glucose was first built based on glucose-depleted human sera. The collected serum samples were pre-treated with GOx to deplete the inherent glucose, and then N-ethylmaleimide was added to eliminate the interference from thiols and mercapto compounds. The treated sera were then incubated with ligand-free UCNPs (0.4 mg·mL^{-1}), DA (500 μM), GOx (0.05 mg·mL^{-1}), and different amounts (0–300 μM) of glucose. After incubation at 37 ℃ for 1 h, the microplate was subjected to UCL measurement under 980-nm excitation. For accurate glucose detection in real serum and whole blood, the samples were pre-treated with N-ethylmaleimide and diluted by 100-fold with Tris-HCl buffer solution. Three independent experiments were carried out to yield the average value and standard deviation. All the UCL measurements for glucose detection were conducted

under 980-nm excitation on the customized UCL biodetection system.

2.7 Characterization

Powder X-ray diffraction (XRD) patterns of the samples were collected using an X-ray diffractometer (MiniFlex II, Rigaku) with Cu Kα1 radiation (λ = 0.154187 nm). Both the low- and high-resolution transmission electron microscopy (TEM) measurements were performed using a Tecnai G^2 F20 TEM equipped with an energy dispersive X-ray spectrum (EDS). Fourier transform infrared (FTIR) spectra were recorded as KBr discs on a Magna 750 FTIR spectrometer. The zeta potential and hydrodynamic diameter distribution of ligand-free UCNPs dispersed in distilled water (pH 6.9) were determined using dynamic light scattering (DLS) measurements (Nano ZS ZEN3600, Malvern). Thermogravimetric analyses (TGA) were conducted on a Netzsch STA449C thermal analysis system under N_2 atmosphere flow at a rate of 10 K·min^{-1}. UC emission spectra were recorded on a spectrometer (FLS980, Edinburgh Instrument) under 980-nm excitation with a continuous-wave diode laser. UCL lifetimes were measured using a customized ultraviolet (UV) to mid-infrared steady-state and phosphorescence lifetime spectrometer (FSP920-C, Edinburgh Instrument) equipped with a digital oscilloscope (TDS3052B, Tektronix) and a tunable mid-band optical parametric oscillator (OPO) pulse laser as the excitation source (410–2,400 nm, 10 Hz, pulse width ≤ 5 ns, Vibrant 355II, OPOTEK). All the spectral data collected were corrected for the spectral response of the spectrometer.

3 Results and Discussion

3.1 Principle for glucose detection based on the UCNPs-PDA bioassay nanosystem

The principle for glucose detection is illustrated in Scheme 1. Ligand-free $NaYF_4$:Yb/Er UCNPs were selected as energy donors in view of the high UC efficiency of $NaYF_4$:Yb/Er and the high affinity of ligand-free UCNPs with DA monomers [37]. The bared Ln^{3+} ions exposed on the surface of ligand-free UCNPs enabled DA monomers to spontaneously attach onto the surface of UCNPs through electrostatic

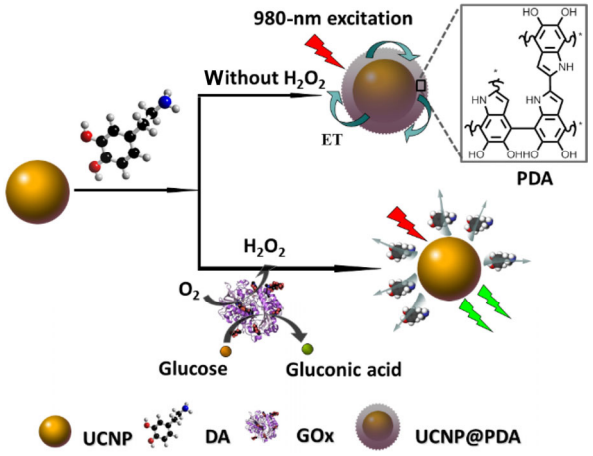

Scheme 1 Schematic illustration of the principle for the detection of H_2O_2 and glucose based on a UCNPs-PDA bioassay nanosystem.

attraction or the strong chelation of Ln^{3+} [38], which further polymerized to form a PDA shell around the UCNPs. PDA exhibits high absorbance in the visible spectral region and thus can function as an effective energy quencher for UCNPs through either FRET or the "inner filter effect" (namely, irradiation/reabsorption) [15]. In the presence of H_2O_2, the polymerization of DA monomers can be inhibited, leading to intense UCL from UCNPs under 980-nm laser excitation. Based on this principle, the UCNPs-PDA nanosystem can be explored as an effective bioassay nano-platform for the detection of H_2O_2 or H_2O_2-generated biomolecules such as glucose that can yield H_2O_2 through the GOx/glucose enzymatic reaction [39, 40]. As a result, the concentration of glucose can be quantified by the UCL intensity of the UCNPs-PDA nanosystem under 980-nm excitation upon adding glucose and GOx.

3.2 Synthesis and characterization of PDA-capped UCNPs

Figure 1(a) depicts the synthesis procedure for PDA-capped UCNPs. Hydrophobic and oleate-capped $NaYF_4$:Yb/Er UCNPs were first synthesized via a high-temperature co-precipitation method. A TEM image (Fig. 1(b)) showed that the as-synthesized UCNPs were roughly spherical with an average diameter of 23.2 ± 0.6 nm. XRD, HRTEM, EDS, and SAED patterns (Figs. S1 and S2 in the Electronic Supplementary Material (ESM)) confirmed the high crystallinity and hexagonal phase of the resulting $NaYF_4$:Yb/Er UCNPs.

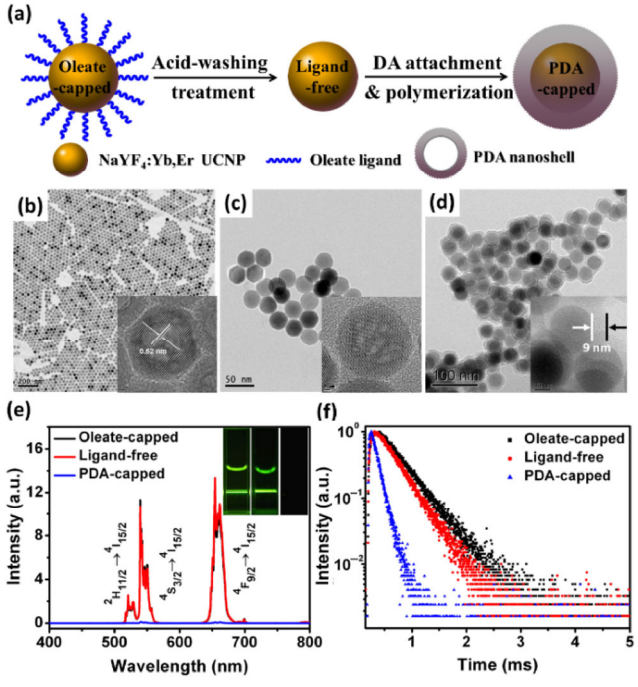

Figure 1 (a) Schematic illustration of the synthetic procedure for PDA-capped UCNPs. TEM and HRTEM images of (b) oleate-capped, (c) ligand-free, and (d) PDA-capped $NaYF_4$:Yb/Er UCNPs. (e) UCL spectra of oleate-capped, ligand-free, and PDA-capped $NaYF_4$:Yb/Er UCNPs under 980-nm excitation. The inset shows the corresponding UCL photographs for a colloidal solution of the UCNPs (2 mg·mL^{-1}) under 980-nm laser irradiation at a power density of 10 W·cm^{-2}. (f) The corresponding UCL decays from $^4S_{3/2}$ by monitoring the Er^{3+} emission at 539 nm.

UCL spectra of the UCNPs (Fig. 1(e)) exhibited sharp and characteristic emission peaks at 521, 539, and 654 nm, which can be assigned to the $^2H_{11/2}$, $^4S_{3/2}$, and $^4F_{9/2} \rightarrow {}^4I_{15/2}$ transitions of Er^{3+}, respectively.

To obtain hydrophilic and ligand-free UCNPs, we removed the surface ligands of the oleate-capped UCNPs through an acid-washing treatment [15, 36]. FTIR spectra and TGA curves (Figs. S3 and S4 in the ESM) confirmed the successful removal of surface ligands. As a result, these ligand-free UCNPs exhibited excellent water solubility and inherited the size and morphology of oleate-capped UCNPs (Fig. 1(b), Figs. S5 and S6 in the ESM). More importantly, the ligand-free UCNPs preserved the intense UCL from their parent oleate-capped UCNPs with nearly unchanged UCL intensity and slightly shortened UCL lifetimes from 466 to 396 μs for $^4S_{3/2}$ and 684 to 678 μs for $^4F_{9/2}$ (Figs. 1(e) and 1(f), and Fig. S7 in the ESM). In addition, owing to the removal of surface ligands, positively charged Ln^{3+} ions were exposed on the surface of ligand-free UCNPs, resulting in a positive zeta potential of +30.5 mV for their colloidal solution at pH 8.5 (Fig. S8 in the ESM). As a consequence, these ligand-free UCNPs were enabled for direct conjugation with electronegative groups of hydrophilic and biocompatible molecules for various bioapplications [41].

Owing to the high affinity of bared Ln^{3+} ions on the surface of ligand-free UCNPs, DA monomers can spontaneously attach onto the surface of UCNPs through electrostatic attraction or the strong chelation of Ln^{3+} [42], facilitating the formation of a PDA shell around UCNPs. The UCNPs@PDA core/shell nanostructures can be clearly distinguished in a TEM image (Fig. 1(d)), where the darker regions correspond to UCNP cores and the brighter regions correspond to PDA shells. As shown in Fig. 2(a), the absorption band of PDA overlaps well with the emission bands of UCNPs, thereby enabling efficient FRET from UCNPs to PDA. As a consequence, under 980-nm excitation, the integrated UCL intensity of PDA-capped UCNPs decreased markedly relative to that of ligand-free UCNPs. Typically, after coating with a

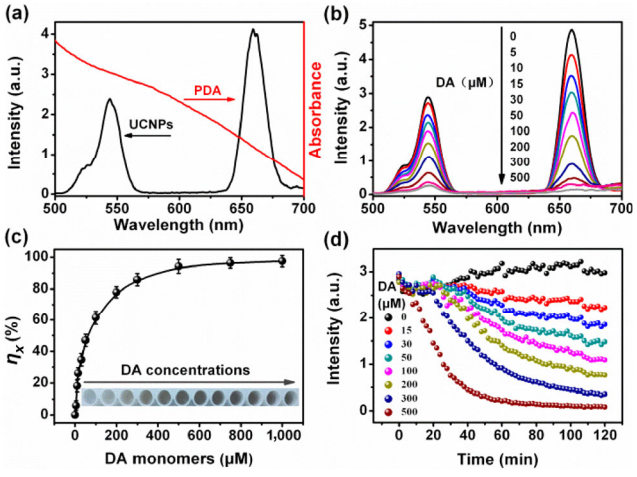

Figure 2 (a) Absorption spectrum of PDA and UCL spectrum of ligand-free $NaYF_4$:Yb/Er UCNPs. (b) DA-concentration–dependent UCL spectra of UCNPs/DA in Tris-HCl buffer solution (pH = 8.5) under 980-nm excitation. (c) UCL quenching efficiency (η_x) for UCNP/DA solution as a function of DA concentration. The inset shows the corresponding photographs for the UCNP/DA solution in a 96-well microplate under day-light. (d) UCL kinetic curves showing the temporal response of the UCL signal at 539 nm for the UCNP/DA solution upon addition of different amounts of DA monomers.

9-nm thick PDA shell, the integrated UCL intensity of the UCNPs decreased by a factor of 115 (Fig. 1(e)), and their UCL lifetimes shortened from 396 to 127 μs for $^4S_{3/2}$ and 678 to 229 μs for $^4F_{9/2}$ (Fig. 1(f) and Fig. S7 in the ESM). Such remarkable decrease in UCL intensity and UCL lifetime unambiguously corroborated the efficient FRET process from the UCNP core to the PDA shell. It is worth mentioning that the PDA layer was stable and barely affected by the photothermal effect, which can be verified by the nearly unchanged absorption of the PDA-capped UCNPs upon irradiation with a 980-nm laser even for a long time of 30 min at a power density of 10 W·cm^{-2} (Fig. S9 in the ESM).

3.3 Quenching effect of PDA on the UCL of UCNPs

To gain more insight into the quenching effect of PDA on the UCL of UCNPs, we evaluated the spectral and temporal response of the UCL upon addition of different amounts of DA monomers (0–1 mM) into aqueous solutions of ligand-free UCNPs (0.4 mg·mL^{-1}). Upon increasing the concentrations of DA monomers, the thickness of the PDA shell around the UCNPs was observed to increase accordingly (Fig. S10 in the ESM), which resulted in enhanced absorption by the PDA shell (Fig. S11 in the ESM). As a result, under 980-nm excitation, the integrated UCL intensity of the UCNPs/DA solution decreased gradually with the increase of DA monomers (Fig. 2(b)), due to the enhanced energy transfer from UCNPs to PDA (Fig. S12 in the ESM).

From UCL spectra, the quenching efficiency (η_x) of PDA on UCL can be calculated by

$$\eta_x = (I_0 - I_x)/I_0 \quad (1)$$

where I_0 and I_x represent the integrated UCL intensity of UCNPs in the absence and presence of x μM of DA monomers, respectively. As shown in Fig. 2(c), the quenching efficiency increased steadily with DA monomers, along with a color change of the UCNPs/DA solution from colorless to dark brown. Typically, when 1 mM of DA monomers were added, the quenching efficiency reached a plateau of 97.4%, which is the highest among those of UC-FRET pairs ever reported [26–28, 43–45]. Such high quenching efficiency of the system can be ascribed to the close proximity between the UCNP core and the PDA shell without any interlayer, which highly promoted the distance-dependent FRET process [42]. Note that not only the FRET process but also the reabsorption of PDA (or the so-called "inner filter effect") contributed to the remarkable UCL quenching of the system [46, 47]. The UCL kinetic curves (Fig. 2(d)), obtained by monitoring the Er^{3+} emission at 539 nm, showed that the UCL of the UCNPs/DA solution exhibited a fast response to the added DA monomers and could stabilize within 2 h, which agreed well with the absorption kinetics of PDA (Fig. S11 in the ESM). Such high quenching efficiency and fast UCL response of the UCNPs-PDA nanosystem are particularly important for their applications in UC-FRET bioassays.

3.4 Inhibition effect of H_2O_2 on UCL quenching of the UCNPs-PDA nanosystem

H_2O_2 in alkaline solution can produce hydroxyl radicals, which are efficient inhibitors to the polymerization reaction of DA monomers via the addition of hydroxyl groups to 5,6-dihydroxyindole (precursor of PDA) [48]. Thus, H_2O_2 may effectively prevent DA monomers from polymerizing into PDA, and thus inhibit the UCL quenching of the UCNPs-PDA nanosystem. Such an inhibition effect can be evidenced by the drastically distinct absorbance and UCL of the UCNPs/DA solution in the absence and presence of H_2O_2. In the absence of H_2O_2, DA monomers can spontaneously attach to the surface of UCNPs and polymerize to form a PDA shell, resulting in the high absorbance of PDA in visible region and significant UCL quenching of the UCNPs/DA solution (Figs. 3(a) and 3(b)). Whereas, in the presence of H_2O_2, the polymerization of DA monomers was inhibited, leading to the decrease of PDA absorption and the recovery of the UCL of the UCNPs/DA solution (Figs. 3(a) and 3(b)).

As expected, the inhibition of H_2O_2 on UCL quenching of the UCNPs-PDA nanosystem relied heavily on the concentration of H_2O_2, thereby paving a new way for the sensitive detection of H_2O_2. Under 980-nm excitation, the integrated UCL intensity of the UCNPs/DA/H_2O_2 solution was observed to increase linearly with the concentration of H_2O_2 from 0–250 μM (Figs. 3(c) and 3(d)), due to gradually alleviated UCL quenching arising from the decreased PDA amounts decorated on the surface of the UCNPs. The limit of

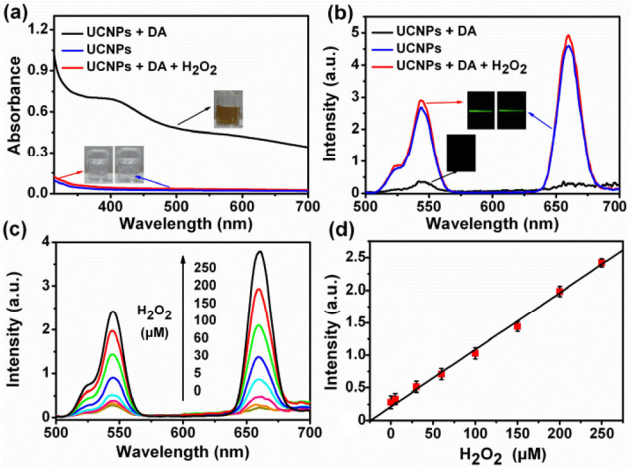

Figure 3 (a) Absorption and (b) UCL spectra of ligand-free $NaYF_4$:Yb/Er UCNPs, UCNPs/DA, and UCNPs/DA/H_2O_2 in Tris-HCl buffer solution (pH = 8.5). The concentrations of UCNPs, DA, and H_2O_2 were 0.4 mg·mL^{-1}, 500, and 300 μM, respectively. The insets show the corresponding photographs of the solutions under (a) day-light and (b) 980-nm excitation. (c) H_2O_2-concentration–dependent UCL spectra of a UCNPs/DA/H_2O_2 solution under 980-nm excitation. (d) Calibration curve for the detection of H_2O_2: Integrated UCL intensity (500–700 nm) vs. concentration of H_2O_2. Each data point represents the mean (± standard deviation) of three independent experiments.

detection (LOD), defined as the concentration that corresponds to three times the standard deviation above the signal measured in the blank, was determined to be 0.75 μM. Such a low LOD can be attributed to the combined advantages of the background-free signal from NIR-triggered UCL and the high UCL quenching efficiency of the UCNPs@PDA core/shell nanostructure. Therefore, the UCNPs-PDA nanosystem can be exploited as a sensitive UC-FRET nanoplatform in a quenching/inhibition format for the detection of H_2O_2 and H_2O_2-generated biomolecules.

3.5 Glucose detection based on the UCNPs-PDA nanosystem

By utilizing the H_2O_2-responsive UCL, we explored the UCNPs-PDA nanosystem which can yield H_2O_2 through the GOx/glucose enzymatic reaction for the sensitive detection of glucose. Note that sole glucose or GOx showed little optical response to the UCNPs-PDA nanosystem, given that no H_2O_2 was generated (Fig. S13 in the ESM). The color of the UCNPs/DA solution remained dark brown upon addition of sole glucose or GOx, whereas it turned colorless when both glucose and GOx were added (Fig. 4(a)). To guarantee the best performance of the detection, the concentrations of UCNPs, DA, and GOx in the detection system were optimized to be 0.4 mg·mL^{-1}, 500 μM, and 0.05 mg·mL^{-1}, respectively, by balancing both the highest UCL quenching and inhibition capability of the system (Fig. 2(c) and Fig. S14 in the ESM). Therefore, glucose can be quantified by measuring the UCL signal of the optimal UCNPs/DA/GOx solution under 980-nm excitation upon addition of glucose into the solution. It was observed that the integrated UCL intensity of the UCNPs/DA/GOx/glucose solution increased linearly with the glucose concentration from 0–300 μM (Figs. 4(b) and 4(c)), due to the gradual release of H_2O_2, which can alleviate the UCL quenching. From the calibration curve (Fig. 4(c)), the LOD was determined to be 0.8 μM, which is much lower than the normal glucose level in human blood (3.6–6.6 mM) [1].

To verify the specificity of the assay, we carried out a control experiment by replacing glucose with other possible interfering biomolecules and electrolytes that exist in complex biological samples, including carbohydrates, proteins, amino acids, and metal ions,

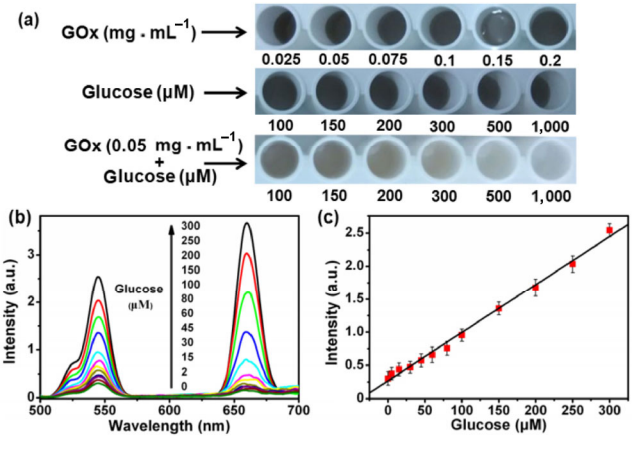

Figure 4 (a) Photograph of UCNPs/DA solution in 96-well microplates under day-light upon addition of different amount of GOx, glucose, or combination of them. The concentrations of UCNPs and DA were 0.4 mg·mL^{-1} and 500 μM, respectively. (b) Glucose-concentration-dependent UCL spectra of UCNPs/DA/GOx/glucose solution under 980-nm excitation. (c) Calibration curve for the detection of glucose: integrated UCL intensity (500–700 nm) vs. glucose concentration. Each data point represents the mean (± standard deviation) of three independent experiments.

under otherwise identical conditions. As shown in Fig. 5, the UCL signal in control groups was negligibly weak, which was in marked contrast to the intense UCL in the experiment group. Such an exclusively intense UCL signal in the experiment group confirmed the high selectivity and specificity of the assay, thereby validating the applicability of the UCNPs-PDA nanosystem for glucose detection in complex biological samples, such as serum and whole blood.

Furthermore, for the detection of glucose in human serum and whole blood, we determined the glucose concentration by measuring the UCL signal in a serum-based detection system and built the calibration curve upon addition of UCNPs/DA/GOx and different amounts of glucose into the glucose-depleted human sera. The UCL signal of the serum-base detection system exhibited a linear dependence on the glucose concentration ranging from 0–250 μM, with an LOD of 1.2 μM (Fig. S15 in the ESM). As a result, the blood glucose levels in human serum and whole blood samples can be determined by measuring the UCL signal of the samples upon addition of UCNPs/DA/GOx. To verify the accuracy and precision of the assay, we further determined the glucose level, coefficient of variation (CV), and the recovery of two human serum samples and one whole blood sample upon addition of different concentrations of glucose. The CVs of all assays were below 8.6% and the recoveries were in the range of 95.2%–107.4% (Table 1), both of which are within the acceptance criteria (CVs ≤ 15%; recoveries in the range of 90%–110%) set for bioanalytical method validation [49]. These results show that the UCNPs-PDA nanosystem has high sensitivity and reliability for blood glucose detection in complex biological samples. Compared to the previously reported UC-FRET bioassay systems [25–28, 50], the UCNPs-PDA nanosystem is much more convenient and cost-effective, given that the assay is performed based on a simple blending of the test samples with ligand-free UCNPs and commercially available DA and GOx and involves no complicated operations in nanoprobe preparation or surface modification. Therefore, the designed UCNPs-PDA nanosystem, containing background-free UCL under NIR excitation and high FRET efficiency within UCNPs@PDA core/shell nanostructures, is highly desired as a homogenous UC-FRET bioassay nanoplatform for the accurate detection of blood glucose or other H_2O_2-generated biomolecules in clinical bioassays.

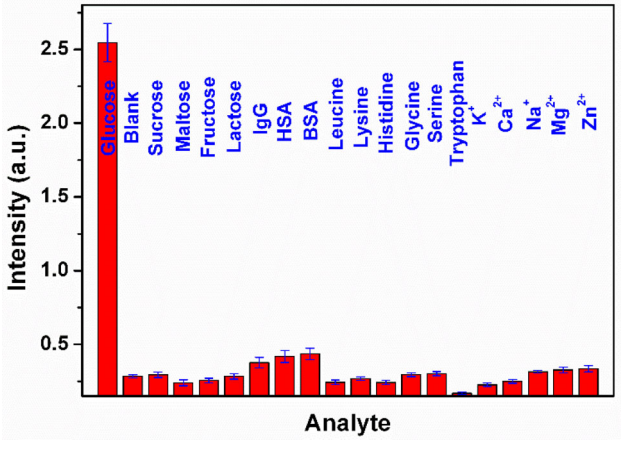

Figure 5 UCL signal at 539 nm of the UCNPs/DA/GOx solution under 980-nm excitation after incubation with 1 mM of different sugars, proteins, L-amino acids, and metal ions. Error bars represent the standard deviations of three independent experiments.

Table 1 Assay precision and analytical recovery of the blood glucose levels in human serum and whole blood, based on a UCNPs-PDA nanosystem

Added (mM)	Found (mM)	CV (%) (n = 4)	Recovery (%)
Serum 1	5.583		—
0.5	6.095	6.17	102.4
1	6.537	5.39	95.40
5	10.79	2.86	104.2
Serum 2	6.347		—
0.5	6.884	6.93	107.4
1	7.412	5.76	106.5
5	11.26	4.49	98.34
Whole blood 3	4.796		—
0.5	5.272	8.56	95.20
1	5.779	5.79	98.30
5	9.628	3.37	96.64

4 Conclusions

In summary, we have developed a facile and cost-effective UC-FRET bioassay nanoplatform for the accurate detection of glucose in human serum and whole blood by employing ligand-free $NaYF_4$:Yb/Er

UCNPs as an energy donor and PDA as an energy quencher. The high absorbance of PDA and the extremely close proximity between the UCNP core and the PDA shell enabled highly efficient FRET from UCNPs to PDA under 980-nm excitation, resulting in remarkable UCL quenching of the UCNPs-PDA nanosystem with an energy transfer efficiency of 97.4%. The formation of the PDA shell and the resulting UCL quenching can be effectively inhibited by H_2O_2 produced via the GOx/glucose enzymatic reaction. Based on such H_2O_2-responsive UCL of the UCNPs-PDA nanosystem, we achieved an LOD of 1.2 μM for glucose detection in human serum and whole blood with high accuracy and reliability. These findings reveal the great potential of the UCNPs-PDA nanosystem for detection of H_2O_2-generated biomolecules in clinical bioassays. The proposed strategy for designing the UCNPs-PDA nanosystem through direct mixing of ligand-free UCNPs with commercially available and cheap chemicals can be extended to other kinds of UC-FRET nanosystems, thereby opening up a new avenue for the exploration of Ln^{3+}-doped UCNPs in versatile bioapplications, such as *in-vitro* detection of serum biomarkers for disease diagnosis and management.

Acknowledgements

This work is supported by the National Basic Research Program of China (973 Program) (No. 2014CB845605), the National Natural Science Foundation of China (NSFC) (Nos. U1305244, 21325104, 51402294 and 21501180), the CAS/SAFEA International Partnership Program for Creative Research Teams, Strategic Priority Research Program of the CAS (Nos. XDA09030307 and XDB20000000), the Youth Innovation Promotion Association (No. 2016277) and the Chunmiao Project of Haixi Institute of the CAS (No. CMZX-2016-002), and the Natural Science Foundation of Fujian Province (Nos. 2015J05116, 2017J05095, 2017J01105 and 2017I0018).

Electronic Supplementary Material: Supplementary material (TEM images, XRD pattern, EDS pattern, FTIR spectra, TGA curves, zeta potential, absorption spectra and UCL decay curves of the UCNPs with different surface structures) is available in the online version of this article at https://doi.org/10.1007/s12274-017-1721-1.

References

[1] Heller, A.; Feldman, B. Electrochemical glucose sensors and their applications in diabetes management. *Chem. Rev.* **2008**, *108*, 2482–2505.

[2] Harris, M. Classification and diagnosis of diabetes mellitus and other categories of glucose intolerance. *Diabetes* **1979**, *28*, 1039–1057.

[3] American Diabetes Association. Diagnosis and classification of diabetes mellitus. *Diabetes Care* **2014**, *37*, S81–S90.

[4] Alberti, K. G. M. M.; Zimmet, P. Z.; Consultation, W. Definition, diagnosis and classification of diabetes mellitus and its complications. Part 1: Diagnosis and classification of diabetes mellitus. Provisional report of a WHO consultation. *Diabet. Med.* **1998**, *15*, 539–553.

[5] Xiong, Y. M.; Zhang, Y. Y.; Rong, P. F.; Yang, J.; Wang, W.; Liu, D. B. A high-throughput colorimetric assay for glucose detection based on glucose oxidase-catalyzed enlargement of gold nanoparticles. *Nanoscale* **2015**, *7*, 15584–15588.

[6] Clarke, S. E.; Foster, J. R. A history of blood glucose meters and their role in self-monitoring of diabetes mellitus. *Br. J. Biomed. Sci.* **2012**, *69*, 83–93.

[7] Trajanoski, Z.; Brunner, G. A.; Gfrerer, R. J.; Wach, P.; Pieber, T. R. Accuracy of home blood glucose meters during hypoglycemia. *Diabetes Care* **1996**, *19*, 1412–1415.

[8] Liu, Q. Y.; Yang, Y. T.; Li, H.; Zhu, R. R.; Shao, Q.; Yang, S. G.; Xu, J. J. NiO nanoparticles modified with 5,10,15,20-tetrakis(4-carboxylpheyl)-porphyrin: Promising peroxidase mimetics for H_2O_2 and glucose detection. *Biosens. Bioelectron.* **2015**, *64*, 147–153.

[9] Zhang, J. X.; Tu, L. P.; Zhao, S.; Liu, G. H.; Wang, Y. Y.; Wang, Y.; Yue, Z. Fluorescent gold nanoclusters based photoelectrochemical sensors for detection of H_2O_2 and glucose. *Biosens. Bioelectron.* **2015**, *67*, 296–302.

[10] Lu, L. F.; Li, Y. Y.; Zhang, M.; Shi, G. Y. Visual fluorescence detection of H_2O_2 and glucose based on "molecular beacon"-hosted Hoechst dyes. *Analyst* **2015**, *140*, 3642–3647.

[11] Liu, B. W.; Sun, Z. Y.; Huang, P. J. J.; Liu, J. W. Hydrogen peroxide displacing DNA from nanoceria: Mechanism and detection of glucose in serum. *J. Am. Chem. Soc.* **2015**, *137*, 1290–1295.

[12] Wang, D.; Wang, R. H.; Liu, L. J.; Qu, Y.; Wang, G. F.; Li, Y. D. Down-shifting luminescence of water soluble $NaYF_4:Eu^{3+}$@Ag core-shell nanocrystals for fluorescence turn-on detection of glucose. *Sci. China Mater.* **2017**, *60*, 68–74.

[13] Medintz, I. L.; Uyeda, H. T.; Goldman, E. R.; Mattoussi, H. Quantum dot bioconjugates for imaging, labelling and sensing. *Nat. Mater.* **2005**, *4*, 435–446.

[14] Resch-Genger, U.; Grabolle, M.; Cavaliere-Jaricot, S.; Nitschke, R.; Nann, T. Quantum dots versus organic dyes as fluorescent labels. *Nat. Methods* **2008**, *5*, 763–775.

[15] Zheng, W.; Huang, P.; Tu, D. T.; Ma, E.; Zhu, H. M.; Chen, X. Y. Lanthanide-doped upconversion nano-bioprobes: Electronic structures, optical properties, and biodetection. *Chem. Soc. Rev.* **2015**, *44*, 1379–1415.

[16] Wang, J. W.; Tanner, P. A. Upconversion for white light generation by a single compound. *J. Am. Chem. Soc.* **2010**, *132*, 947–949.

[17] Zhou, B.; Shi, B. Y.; Jin, D. Y.; Liu, X. G. Controlling upconversion nanocrystals for emerging applications. *Nat. Nanotechnol.* **2015**, *10*, 924–936.

[18] Su, Q. Q.; Feng, W.; Yang, D. P.; Li, F. Y. Resonance energy transfer in upconversion nanoplatforms for selective biodetection. *Acc. Chem. Res.* **2017**, *50*, 32–40.

[19] Tsang, M. K.; Ye, W. W.; Wang, G. J.; Li, J. M.; Yang, M.; Hao, J. H. Ultrasensitive detection of ebola virus oligonucleotide based on upconversion nanoprobe/nanoporous membrane system. *ACS Nano* **2016**, *10*, 598–605.

[20] Liu, Y. Y.; Zhang, J. W.; Zuo, C. J.; Zhang, Z.; Ni, D. L.; Zhang, C.; Wang, J.; Zhang, H.; Yao, Z. W.; Bu, W. B. Upconversion nano-photosensitizer targeting into mitochondria for cancer apoptosis induction and cyt c fluorescence monitoring. *Nano Res.* **2016**, *9*, 3257–3266.

[21] Xu, W.; Zhu, Y. S.; Chen, X.; Wang, J.; Tao, L.; Xu, S.; Liu, T.; Song, H. W. A novel strategy for improving upconversion luminescence of $NaYF_4$:Yb,Er nanocrystals by coupling with hybrids of silver plasmon nanostructures and poly(methyl methacrylate) photonic crystals. *Nano Res.* **2013**, *6*, 795–807.

[22] Huang, P.; Tu, D. T.; Zheng, W.; Zhou, S. Y.; Chen, Z.; Chen, X. Y. Inorganic lanthanide nanoprobes for background-free luminescent bioassays. *Sci. China Mater.* **2015**, *58*, 156–177.

[23] Luo, W. Q.; Liu, Y. S.; Chen, X. Y. Lanthanide-doped semiconductor nanocrystals: Electronic structures and optical properties. *Sci. China Mater.* **2015**, *58*, 819–850.

[24] Lu, S.; Tu, D. T.; Li, X. J.; Li, R. F.; Chen, X. Y. A facile "ship-in-a-bottle" approach to construct nanorattles based on upconverting lanthanide-doped fluorides. *Nano Res.* **2016**, *9*, 187–197.

[25] Liu, J. L.; Lu, L. L.; Li, A. Q.; Tang, J.; Wang, S. G.; Xu, S. Y.; Wang, L. Y. Simultaneous detection of hydrogen peroxide and glucose in human serum with upconversion luminescence. *Biosens. Bioelectron.* **2015**, *68*, 204–209.

[26] Yuan, J.; Cen, Y.; Kong, X. J.; Wu, S.; Liu, C. L.; Yu, R. Q.; Chu, X. MnO_2-nanosheet-modified upconversion nanosystem for sensitive turn-on fluorescence detection of H_2O_2 and glucose in blood. *ACS Appl. Mater. Interfaces* **2015**, *7*, 10548–10555.

[27] Wu, S.; Kong, X. J.; Cen, Y.; Yuan, J.; Yu, R. Q.; Chu, X. Fabrication of a LRET-based upconverting hybrid nanocomposite for turn-on sensing of H_2O_2 and glucose. *Nanoscale* **2016**, *8*, 8939–8946.

[28] Zhang, C. L.; Yuan, Y. X.; Zhang, S. M.; Wang, Y. H.; Liu, Z. H. Biosensing platform based on fluorescence resonance energy transfer from upconverting nanocrystals to graphene oxide. *Angew. Chem., Int. Ed.* **2011**, *50*, 6851–6854.

[29] Lee, H.; Dellatore, S. M.; Miller, W. M.; Messersmith, P. B. Mussel-inspired surface chemistry for multifunctional coatings. *Science* **2007**, *318*, 426–430.

[30] Ku, S. H.; Park, C. B. Human endothelial cell growth on mussel-inspired nanofiber scaffold for vascular tissue engineering. *Biomaterials* **2010**, *31*, 9431–9437.

[31] Kang, S. M.; You, I.; Cho, W. K.; Shon, H. K.; Lee, T. G.; Choi, I. S.; Karp, J. M.; Lee, H. One-step modification of superhydrophobic surfaces by a mussel-inspired polymer coating. *Angew. Chem., Int. Ed.* **2010**, *49*, 9401–9404.

[32] Liu, Y. L.; Ai, K. L.; Lu, L. H. Polydopamine and its derivative materials: Synthesis and promising applications in energy, environmental, and biomedical fields. *Chem. Rev.* **2014**, *114*, 5057–5115.

[33] Swan, G. A. Chemical structure of melanins. *Ann. N. Y. Acad. Sci.* **1963**, *100*, 1005–1019.

[34] Qiang, W. B.; Li, W.; Li, X. Q.; Chen, X.; Xu, D. K. Bioinspired polydopamine nanospheres: A superquencher for fluorescence sensing of biomolecules. *Chem. Sci.* **2014**, *5*, 3018–3024.

[35] Tu, D. T.; Liu, Y. S.; Zhu, H. M.; Li, R. F.; Liu, L. Q.; Chen, X. Y. Breakdown of crystallographic site symmetry in lanthanide-doped $NaYF_4$ crystals. *Angew. Chem., Int. Ed.* **2013**, *52*, 1128–1133.

[36] Bogdan, N.; Vetrone, F.; Ozin, G. A.; Capobianco, J. A. Synthesis of ligand-free colloidally stable water dispersible brightly luminescent lanthanide-doped upconverting nanoparticles. *Nano Lett.* **2011**, *11*, 835–840.

[37] Krämer, K. W.; Biner, D.; Frei, G.; Güdel, H. U.; Hehlen, M. P.; Lüthi, S. R. Hexagonal sodium yttrium fluoride based green and blue emitting upconversion phosphors. *Chem. Mater.* **2004**, *16*, 1244–1251.

[38] Huang, P.; Zheng, W.; Zhou, S. Y.; Tu, D. T.; Chen, Z.; Zhu, H. M.; Li, R. F.; Ma, E.; Huang, M. D.; Chen, X. Y. Lanthanide-doped $LiLuF_4$ upconversion nanoprobes for the detection of disease biomarkers. *Angew. Chem., Int. Ed.*

2014, *53*, 1252–1257.

[39] Wong, C. M.; Wong, K. H.; Chen, X. D. Glucose oxidase: Natural occurrence, function, properties and industrial applications. *Appl*. *Microbiol*. *Biotechnol*. **2008**, *78*, 927–938.

[40] Shan, C. S.; Yang, H. F.; Song, J. F.; Han, D. X.; Ivaska, A.; Niu, L. Direct electrochemistry of glucose oxidase and biosensing for glucose based on graphene. *Anal*. *Chem*. **2009**, *81*, 2378–2382.

[41] Zheng W.; Zhou S. Y.; Xu J.; Liu Y. S.; Huang P.; Liu Y.; Chen X. Y. Ultrasensitive luminescent *in vitro* detection for tumor markers based on inorganic lanthanide nano-bioprobes. *Adv*. *Sci*. **2016**, *3*, 1600197.

[42] Wang, M.; Chen, Z.; Zheng, W.; Zhu, H. M.; Lu, S.; Ma, E.; Tu, D. T.; Zhou, S. Y.; Huang, M. D.; Chen, X. Y. Lanthanide-doped upconversion nanoparticles electrostatically coupled with photosensitizers for near-infrared-triggered photodynamic therapy. *Nanoscale* **2014**, *6*, 8274–8282.

[43] Chen, H. Y.; Fang, A. J.; He, L.; Zhang, Y. Y.; Yao, S. Z. Sensitive fluorescent detection of H_2O_2 and glucose in human serum based on inner filter effect of squaric acid-iron(III) on the fluorescence of upconversion nanoparticle. *Talanta* **2017**, *164*, 580–587.

[44] Xiao, Y.; Zeng, L. Y.; Xia, T.; Wu, Z. J.; Liu, Z. H. Construction of an upconversion nanoprobe with few-atom silver nanoclusters as the energy acceptor. *Angew*. *Chem*., *Int*. *Ed*. **2015**, *54*, 5323–5327.

[45] Li, Z.; Liang, T.; Lv, S. W.; Zhuang, Q. G.; Liu, Z. H. A rationally designed upconversion nanoprobe for *in vivo* detection of hydroxyl radical. *J*. *Am*. *Chem*. *Soc*. **2015**, *137*, 11179–11185.

[46] Achatz, D. E.; Meier, R. J.; Fischer, L. H.; Wolfbeis, O. S. Luminescent sensing of oxygen using a quenchable probe and upconverting nanoparticles. *Angew*. *Chem*., *Int*. *Ed*. **2011**, *50*, 260–263.

[47] Gorris, H. H.; Wolfbeis, O. S. Photon-upconverting nanoparticles for optical encoding and multiplexing of cells, biomolecules, and microspheres. *Angew*. *Chem*., *Int*. *Ed*. **2013**, *52*, 3584–3600.

[48] Lin, J. H.; Yu, C. J.; Yang, Y. C.; Tseng, W. L. Formation of fluorescent polydopamine dots from hydroxyl radical-induced degradation of polydopamine nanoparticles. *Phys*. *Chem*. *Chem*. *Phys*. **2015**, *17*, 15124–15130.

[49] Shah, V. P.; Midha, K. K.; Findlay, J. W. A.; Hill, H. M.; Hulse, J. D.; McGilveray, I. J.; McKay, G.; Miller, K. J.; Patnaik, R. N.; Powell, M. L. et al. Bioanalytical method validation-a revisit with a decade of progress. *Pharm*. *Res*. **2000**, *17*, 1551–1557.

[50] Wang, M.; Li, M.; Yang, M. Y.; Zhang, X. M.; Yu, A. Y.; Zhu, Y.; Qiu, P. H.; Mao, C. B. NIR-induced highly sensitive detection of latent fingermarks by $NaYF_4$: Yb, Er upconversion nanoparticles in a dry powder state. *Nano Res*. **2015**, *8*, 1800–1810.